JAERI-Data/Code--94-017

JP9504223

JAERI-Data/Code 94-017

IMPLICIT TIME-DEPENDENT FINITE DIFFERENT ALGORITHM FOR QUENCH SIMULATION

December 1994

Norikiyo KOIZUMI, Yoshikazu TAKAHASHI and Hiroshi TSUJI

日本原子力研究所
Japan Atomic Energy Research Institute

本レポートは，日本原子力研究所が不定期に公刊している研究報告書です．

入手の問合わせは，日本原子力研究所技術情報部情報資料課（〒319-11 茨城県那珂郡東海村）あて，お申し越しください．なお，このほかに財団法人原子力弘済会資料センター（〒319-11 茨城県那珂郡東海村日本原子力研究所内）で複写による実費頒布をおこなっております．

This report is issued irregularly.

Inquiries about availability of the reports should be addressed to Information Division, Department of Technical Information, Japan Atomic Energy Research Institute, Tokai-mura, Naka-gun, Ibaraki-ken 319-11, Japan.

編集兼発行　日本原子力研究所

印　　刷　㈱原子力資料サービス

Implicit Time-dependent Finite Different Algorithm for Quench Simulation

Norikiyo KOIZUMI, Yoshikazu TAKAHASHI and Hiroshi TSUJI

Department of Fusion Engineering Research
Naka Fusion Research Establishment
Japan Atomic Energy Research Institute
Naka-machi, Naka-gun, Ibaraki-ken

(Received November 4, 1994)

A magnet in a fusion machine has many difficulties in its application because of requirement of a large operating current, high operating field and high breakdown voltage. A cable-in-conduit (CIC) conductor is the best candidate to overcome these difficulties. However, there remained uncertainty in a quench event in the cable-in-conduit conductor because of a difficulty to analyze a fluid dynamics equation. Several scientists, then, developed the numerical code for the quench simulation. However, most of them were based on an explicit time-dependent finite difference scheme. In this scheme, a discrete time increment is strictly restricted by CFL (Courant-Friedrichs-Lewy) condition. Therefore, long CPU time was consumed for the quench simulation. Authors, then, developed a new quench simulation code, POCHI1, which is based on an implicit time dependent scheme. In POCHI1, the fluid dynamics equation is linearlized according to a procedure applied by Beam and Warming and then, a tridiagonal system can be offered. Therefore, no iteration is necessary to solve the fluid dynamics equation. This leads great reduction of the CPU time. Also, POCHI1 can cope with non-linear boundary condition. In this study, comparison with experimental results was carried out. The normal zone propagation behavior was investigated in two samples of CIC conductors which had different hydraulic diameters. The measured and simulated normal zone propagation length showed relatively good agreement. However, the behavior of the normal voltage shows a little disagreement. These results indicate necessity to improve the treatment of the heat transfer coefficient in the turbulent flow region and the electric resistivity of the copper stabilizer in high temperature and high field region.

Keywords: CICC, Quench Simulation, Implicit Time-dependent

陰差分解法によるクエンチ・シミュレーションのアルゴリズム

日本原子力研究所那珂研究所核融合工学部
小泉 徳潔・高橋 良和・辻 博史

（1994年11月4日受理）

核融合炉用超電導コイルは，使用時の運転電流，運転磁場が大きく，また高い絶縁性能が要求されるために，多くの技術的課題を有する。ケーブル・イン・コンジット導体は，これらの問題に対処できる導体として最有力視されている。しかしながら，ケーブル・イン・コンジット導体のクエンチ時の挙動は流体方程式を解かなければならないために，不明な点が残っている。このために，クエンチ・シミュレーション・コードが開発された。しかし，これらのコードは陽解法を基礎にしたため，CFL（クーラン・フリードリクス・レヴィ）条件から時間刻み幅に強い制約を受け，長時間の計算時間が必要とされた。そこで，著者らは陰解法によるクエンチ・シミュレーション・コード（POCHI1）を開発した。POCHI1では，流体方程式をBeamおよびWarmingの用いた線形化手法を用いて線形化した。本線形化により三重対角系得られ，繰り返し計算を行わずに解を求めることができるため，計算時間が大幅に節約できる。本報告書では，計算結果と実験結果の比較も行った。実験では，水力直径の異なる2つのサンプルに対して，クエンチ時の常電導伝播の様子を調査した。計算結果と実験結果は比較的よく一致したが，乱流域での熱伝達率，高温度，高磁場領域での電気抵抗率の取り扱いに多少の問題点が残ることも分かった。

那珂研究所：〒311－01 茨城県那珂郡那珂町大字向山801－1

Contents

目　　次

Nomenclature

t [s]	Time	δt [s]	Discrete time increment
x [m]	Longitudinal length	δx [m]	Discrete length increment
ρ [kg/m^3]	Coolant density	$\dot{m}$ [kg/sm^2]	Coolant mass flow rate
E [J/m^3]	Coolant total internal energy	θ [K]	Strand temperature
ϕ [K]	Conduit temperature	T[K]	Coolant temperature
u [m/s]	Coolant velocity	P[Pa]	Coolant pressure
e [J/m^3]	Coolant internal energy	θ_{cs}[K]	Current sharing temperature
θ_c[K]	Critical temperature	γ [J/m^3]	Coolant heat capacity
γ_{st} [J/m^3]	Heat capacity of strands	γ_{sc}[J/m^3]	Heat capacity of superconductor
γ_{Cu} [J/m^3]	Heat capacity of copper	γ_c [J/m^3]	Heat capacity of conduit
λ [W/mK]	Coolant heat conductance	λ_{Cu} [W/mK]	Thermal conductivity of copper
E_h [J/m^3]	Input energy	t_h [s]	Heating time
Q [W/m^3]	Total heating power	Q_J [W/m^3]	Joule heating power
Q_h [W/m^3]	Input heating power	q [W/m^2]	Heat flux from conductor to coolant
h [W/m^{2}K]	Heat transfer coefficient	h_s [W/m^{2}K]	Steady heat transfer coefficient
h_K [W/m^{2}K]	Kapitza conductance	h_t [W/m^{2}K]	Transient heat transfer coefficient
Re	Reynolds number	Re_c	Critical Reynolds number
Pr	Plandtl number	f	Friction factor
f_l	Laminar friction factor	f_t	Turbulent friction factor
r [Ωm]	Electric resistivity of copper	I_t [A]	Transport current
A_{Cu} [m^2]	Copper cross sectional area	A_{st} [m^2]	Cross sectional area of strands
A_c [m^2]	Conduit cross sectional area	A_{He} [m^2]	Coolant cross sectional area
Pe [m]	Cooling perimeter	D_h [m]	Hydraulic diameter
C_{in}	Flow resistance at inlet	C_{out}	Flow resistance at outlet

1 Introduction

A cable-in-conduit (CIC) superconductor is the best candidate for application to coils in a tokamak fusion reactor because of its high mechanical and electrical insulation performance. Especially, its low loss characteristic is inevitable for the application to a Poloidal field coil. In the CIC conductor, the strands are cooled by supercritical helium (SHe) flowing in the space enclosed by a conduit. Sudden pressure and temperature rise is taken place at a coil quench and then, irreversible damage of the conductor and/or deterioration of electrical insulation performance may be caused. The prediction of the quench behavior is therefore important in coil and conductor designing. It is necessary for this prediction to solve the fluid dynamics equation in the CIC superconductor. Since it is quite difficult to analytically solve the fluid dynamics equation, there remained uncertain in the quench characteristic in the CIC conductor.

Numerical codes have then been developed for the simulation of the quench event by several scientists[1-7]. Most of them are based on the explicit time-dependent finite difference scheme. For the accurate simulation of the quench event, the spatial discrete should be fine on the region where the conductor is normal state and the temperature gradient in the longitudinal direction is large. With the explicit scheme, the spatial discrete strictly restricts the time step from CFL condition[8] and then, quite long CPU time is necessary.

A few scientists[6,7] then developed an implicit time-dependent scheme, which theoretically has no restriction from the CFL condition, to reduce the CPU time. Authors also developed new implicit time dependent code, POCHI1. In this code, the fluid dynamics equation is solved by linearizing according to the linearization procedure applied by Beam and Warming[9]. This linearization offers a tridiagonal system. Consequently, the fluid dynamics equation can be solved without iteration, resulting in much reduction of the CPU time. The algorithm of this code is reported in this paper.

For the verification of applicability of POCHI1, the normal zone propagation behavior was investigated for two CIC superconductors and simulation results were compared with their experimental results. The result of this verification is also described in this paper.

2 Simulation method

2.1 Simulation model and governing equation

2.1.1 Governing equation for the conductor

Since thermal diffusivity of copper stabilizer is quite large compared with these of other material in the strands, the heat conduction in the strands is dominated by the one in the cooper stabilizer. The heat conduction through the other materials is consequently

neglected in the heat conduction equation for the strands. The temperature in the cross-section of the strands is assumed to be uniform because of the good thermal diffusivity of the copper stabilizer. This assumption allows us to treat the heat conduction in the strands as an one dimensional problem. Thus, one has,

$$\gamma_{st} A_{st} \frac{\partial \theta}{\partial t} - A_{Cu} \frac{\partial}{\partial x}\left(\lambda_{Cu} \frac{\partial \theta}{\partial x}\right) + q_{st}^{He} Pe_{st}^{He} + q_{st}^{c} Pe_{st}^{c} - A_{st} Q = 0. \tag{1}$$

Where,

$$A_{st} = A_{Cu} + A_{sc} + A_{el}, \tag{2}$$

$$\gamma_{st} = \frac{A_{Cu}\gamma_{Cu} + A_{sc}\gamma_{sc} + A_{el}\gamma_{el}}{A_{st}}. \tag{3}$$

A_{el}[m^2] and γ_{el}[J/m^{3}K] denote the cross-sectional area and the heat capacity per unit volume of the strands excluding the copper stabilizer and superconductor respectively, if a strand includes other materials except for the superconductor and copper. q_{st}^{He} and q_{st}^{c} denote a heat flux from the strands to the coolant and the conduit, respectively. Pe_{st}^{He} and Pe_{st}^{c} are cooling perimeter of the strands and contact perimeter between the strands and the conduit.

For the conduit, temperature profile in its cross section is also assumed to be uniform since the thickness of the conduit is not so thick in general. Joule heat generation in the conduit at normal transition is neglected, for simplicity, since it is enough small. Thus, the heat conduction equation for the conduit is,

$$\gamma_c A_c \frac{\partial \phi}{\partial t} - A_c \frac{\partial}{\partial x}\left(\lambda_c \frac{\partial \phi}{\partial x}\right) + q_c^{He} Pe_c^{He} - q_{st}^{c} Pe_{st}^{c} = 0. \tag{4}$$

Where q_c^{He} and Pe_c^{He} denote a heat flux from the conduit to the coolant and cooling perimeter of the conduit.

By eliminating a term of $q_{st}^{c} Pe_{st}^{c}$ from Equations (1) and (4), one obtains,

$$\begin{aligned} &\gamma_{st} A_{st} \frac{\partial \theta}{\partial t} + \gamma_c A_c \frac{\partial \phi}{\partial t} - A_{Cu} \frac{\partial}{\partial x}\left(\lambda_{Cu} \frac{\partial \theta}{\partial x}\right) - A_c \frac{\partial}{\partial x}\left(\lambda_c \frac{\partial \phi}{\partial x}\right) \\ &\quad + q_{st}^{He} Pe_{st}^{He} + q_c^{He} Pe_c^{He} - A_{st} Q = 0. \end{aligned} \tag{5}$$

Since the contact perimeter between the strands and the conduit is anticipated to be short in comparison with the cooling perimeter, it is expected that temperature of the conduit is almost equal to the one of the helium during a quench. It is assumed the conduit temperature equals to the helium temperature, for simplicity. Thus, Equation (5) can be rewritten as,

$$\gamma_{st} \frac{\partial \theta}{\partial t} - \frac{A_{Cu}\lambda_{Cu}}{A_{st}} \frac{\partial^2 \theta}{\partial x^2} - \frac{A_{Cu}}{A_{st}} \frac{\partial \lambda_{Cu}}{\partial x} \frac{\partial \theta}{\partial x} + \frac{qPe}{A_{st}} + \frac{\gamma_c A_c}{A_{st}} \frac{\partial T}{\partial t} - Q = 0. \tag{6}$$

Where,

$$q = h(\theta - T). \tag{7}$$

And, Pe_{st}^{He} is substituted by Pe, for simplicity. In Equation (6), the heat conduction in

the conduit is ignored since it is small compared with the one in the copper.

2.1.2 *Governing equation for the coolant*

Conductor length is much longer than the typical length in the cross-section of a conductor, such as a hydraulic diameter and/or a conductor diameter, in a general CIC superconductor. The effect from the distribution of the thermal properties and coolant moment in the cross section is not thought to be dominant in the quench simulation. Therefore, one dimensional model is adopted for the simulation of the coolant behavior to reduce the CPU time and to avoid difficulty included in two or three dimensional problem. Present simulation is carried out for the simplified one dimensional tube model shown in *Figure 1*, neglecting geometrical complexity of the CIC conductor. In this model, the coolant flows in a tube whose inner diameter equals to the hydraulic diameter of the conductor and is heated by the inner surface of the tube. The temperature of the inner surface of the tube is assumed to equal to the strands temperature. The thermal properties and coolant moment are assumed to be uniform in the cross section of the tube. The governing equations for the coolant, therefore, are as follows.

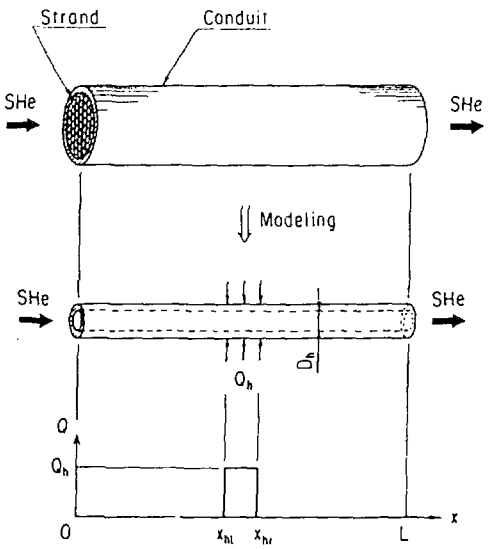

Figure 1. One dimensional tube model for the simulation of the coolant behavior.

$$\frac{\partial \boldsymbol{u}}{\partial t} + \frac{\partial \boldsymbol{F}}{\partial x} + \boldsymbol{G} = \boldsymbol{0} \,. \tag{8}$$

Where,

$$\boldsymbol{u} = \begin{pmatrix} \rho \\ \dot{m} \\ E \end{pmatrix}, \quad \boldsymbol{F} = \begin{pmatrix} \dot{m} \\ \dfrac{\dot{m}^2}{\rho} + P \\ \dfrac{\dot{m}}{\rho}(E+P) \end{pmatrix}, \quad \boldsymbol{G} = \begin{pmatrix} 0 \\ \dfrac{4\tau}{D_h} \\ -\dfrac{Peq}{A_{He}} \end{pmatrix}. \tag{9}$$

$$\tau = \frac{f}{4}\frac{\dot{m}|\dot{m}|}{2\rho}. \tag{10}$$

The heat conduction in helium is neglected in this equation, for simplicity.

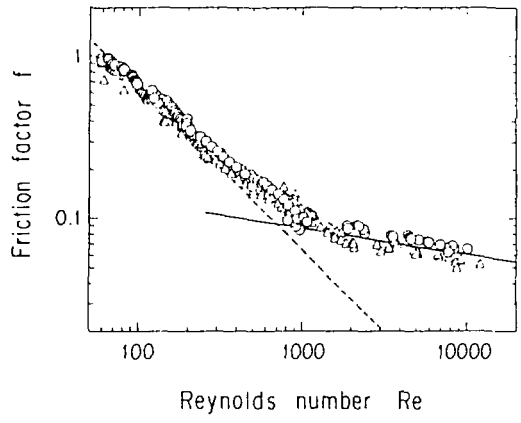

Figure 2. Friction factor measured for two 80 m length CIC conductors. A dot line and a solid line denote the calculated friction factor by Equations (12) and (13), respectively.

2.1.3 Friction factor

The friction factor is calculated with the formula derived from the experiment[10] in which it was measured for two 80 m length CIC conductors. The experimental results are shown in *Figure 2*. The measured friction factor is dominated by a general formula for a laminar flow in a smooth tube on the low Reynolds number region. However, in the high Reynolds number region, the measured friction factor is higher than the one in a smooth tube. The friction factor in the CIC conductors seems to be in accordance of the new formula in this region. The transition from laminar flow to a turbulent flow is not clear in this experiment as well as in the former experiments[11,12]. Therefore, the transition point is supposed to be the intersection of the calculated laminar and turbulent friction factors. The friction factor is then represented as,

$$f = \begin{cases} f_l & (Re \le Re_c) \\ f_t & (Re_c < Re) \end{cases}, \tag{11}$$

Where,

$$f_l = 64/Re\,. \tag{12}$$

$$f = 0.257 Re^{-0.157}\,. \tag{13}$$

The critical Reynolds number is calculated to be about 700.

2.1.4 Heat transfer coefficient

Heat transfer coefficient is calculated from

$$h = \begin{cases} h_K & (t = 0), \\ \dfrac{h_K h_{max}}{h_K + h_{max}} & (t > 0). \end{cases} \tag{14}$$

Kapitza conductance is calculated from the equation in the reference 5. The difference between the conductor temperature and the coolant temperature is ignored since Kapitza conductance plays a role when the temperature difference is small, such as at the begin of

heating. Thus,

$$h_K = 800\theta^3 \ . \tag{15}$$

h_{max} [W/m^{2}K] is calculated from,

$$h_{max} = \mathrm{Max}(h_t, h_s) \ . \tag{16}$$

The signature $\mathrm{Max}(a,b)$ indicates the maximum value between a and b. This equation implies that the steady state heat transfer starts when the fluid boundary layer becomes thinner than the temperature boundary layer[13].

The steady state heat transfer coefficient is calculated from,

$$h_s = \begin{cases} 4\lambda/D_h & (Re \le Re_c), \\ 0.023\lambda Re^{0.8} Pr^{0.4}/D_h & (Re_c < Re). \end{cases} \tag{17}$$

The transient heat transfer characteristic is affected on by temperature profile in the coolant perpendicular to the strand surface. The temperature profile depends on the history of the heat flux from the strand surface and the thickness of the boundary layer. Two or three dimensional simulation would be required for the precise treatment of them. Although POCHI1 is one dimensional code, these effects on the transient heat transfer is taken into account in it from analytic estimation .

It can be assumed that the temperature boundary layer is thinner than the fluid boundary layer during the transient heat transfer[13]. Consequently, the transient heat transfer coefficient can be estimated without taking the effect of the convection in the coolant flow into account. The transient heat transfer coefficient is calculated as the solution of one dimensional heat conduction problem from the heated wall to semi-infinite bath of the coolant under assumption of constant thermal properties, as is assumed in usual estimation of a transient heat transfer coefficient[14,15]. The effect from the heating history and boundary layer are separately considered

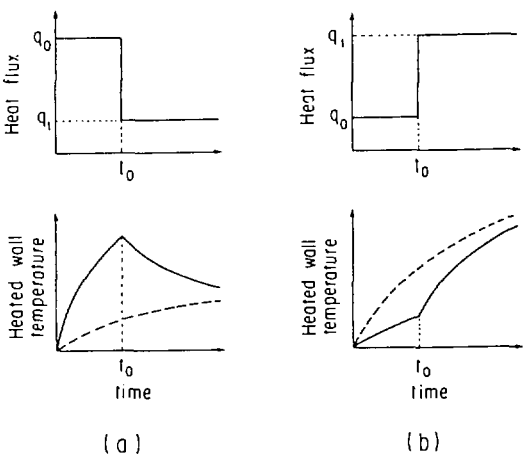

Figure 3. Dependence of transient heat transfer on heating history. (a) Solid and broken lines indicate temperature profiles in cases that heat flux decreases from q_0 to q_1 at $t = t_0$ and the heat flux is q_1 from the beginning of heating, respectively. Temperature of the former case is higher than the latter on the region of $t > t_0$ in spite of same heat flux. (b) Solid and broken lines indicate temperature profiles in cases that heat flux increases from q_0 to q_1 at $t = t_0$ and the heat flux is q_1 from the beginning of heating, respectively. Temperature of former case is lower than the latter on $t > t_0$ in spite of same heat flux.

as follows.

(a) Effect of the heating history.

In case that the heat flux is large till certain time and decreases thereafter, as shown in *Figure 3 (a)*, the coolant near the wall surface is heated hard at first. The warm coolant zone is then formed near the wall surface shown in *Figure 3 (a)*, resulting in degradation of the heat transfer performance. In contrast, when the heat flux increases at certain time, as shown in *Figure 3 (b)*, the cool coolant remains around the wall surface. Consequently, the high heat transfer performance can be obtained, as shown in *Figure 3 (b)*. These two cases correspond to following cases, respectively.

1) The conductor is heated by heat input, such as a disturbance, and Joule heating at first and, thereafter, merely by Joule heating.
2) At normal front region, Joule heating starts after the conductor transits into normal state.

Therefore, it is necessary to take the history of the heating into account in the estimation of the transient heat transfer performance. The transient heat transfer coefficient given with the following equation includes the effect of the history of the heat flux[14].

$$h_t = \frac{\sqrt{\pi\lambda\gamma}\,q(t)}{\int_0^t q(t-\tau)\frac{d\tau}{\tau}} \quad (18)$$

Moreover, this equation can deal with the history of the heat flux which arbitrarily varies relating to time.

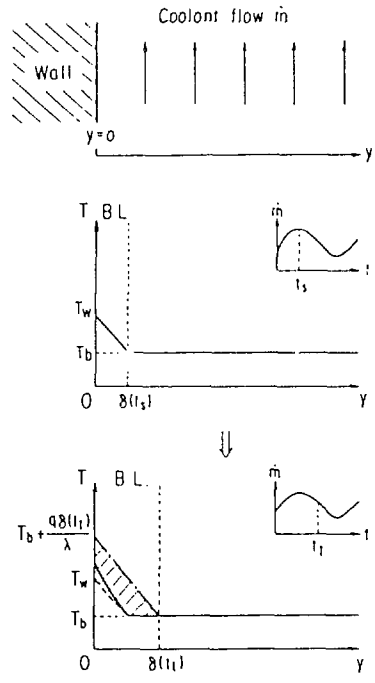

Figure 4. Transient heat transfer after steady heat transfer. The transient heat transfer starts when the steady heat transfer declines as a result of decrease of the coolant flow rate. (a) temperature profile at steady heat transfer. (b) A solid line denotes the temperature profile during the transient heat transfer after the steady heat transfer. A broken and dot-dash line indicate the ones at steady heat transfer before and after flow reduction, respectively. The heat capacity in a shaded area can be used in this transient heat transfer. B.L. in the figure indicates fluid boundary layer.

(b) Effect of the fluid boundary layer.

When the fluid boundary layer becomes thicker than the temperature boundary layer, the steady heat transfer starts. However, if the flow rate declines from certain time of t_s [s], the fluid boundary layer grows. Since cool helium remains in the grown fluid boundary layer, the transient heat transfer owing to this cool helium starts thereafter, as shown in *Figure 4*. The transient heat transfer coefficient in this case is evaluated as follows.

In the turbulent flow, the coolant temperature decreases in the boundary layer and is almost same in the turbulent flow region. It is assumed that the coolant temperature linearly declines from the strand temperature to the bath temperature in the boundary layer, as shown in *Figure 4 (a)*, at the beginning of the coolant flow decrease. Also, it is assumed that the heat flux q [W/m^2] is a constant after the decline of the coolant flow, for simplicity. Thus, the transient heat transfer coefficient can be calculated as the solution of the following equations.

$$\gamma \frac{\partial T}{\partial t} = \lambda \frac{\partial^2 T}{\partial y^2}, \tag{19}$$

$$-\lambda \left.\frac{\partial T}{\partial y}\right|_{y=0} = q, \tag{20}$$

$$T|_{t=0} = \begin{cases} T_w - q_s y/\delta & (0 \le y < \delta) \\ T_b & (\delta \le y) \end{cases}. \tag{21}$$

Where q_s [W/m^2], T_b [K], T_w [K] and δ [m] denote a heat flux at $t = 0$, bath temperature, wall temperature and the thickness of the fluid boundary layer, respectively. The flow reduction is assumed to start at $t = 0$ in this system, for simplicity. The solution of the Equations (19) - (21) is,

$$\begin{aligned} T - T_b = {} & \frac{2(\phi - \phi_s)\sqrt{\kappa t}}{\sqrt{\pi}} e^{-\frac{y^2}{4\kappa t}} + \frac{\phi_s \sqrt{\kappa t}}{\sqrt{\pi}} \left(e^{-\frac{(y+\delta)^2}{4\kappa t}} + e^{-\frac{(y-\delta)^2}{4\kappa t}} \right) \\ & + \frac{\phi_s (y+\delta)}{2} \mathrm{erf}\left(\frac{y+\delta}{2\sqrt{\kappa t}} \right) + \frac{\phi_s (y-\delta)}{2} \mathrm{erf}\left(\frac{y-\delta}{2\sqrt{\kappa t}} \right) \\ & - \phi y \, \mathrm{erfc}\left(\frac{y}{2\sqrt{\kappa t}} \right) - \phi_s y \, \mathrm{erf}\left(\frac{y}{2\sqrt{\kappa t}} \right). \end{aligned} \tag{22}$$

Where $\mathrm{erf}(z)$ and $\mathrm{erfc}(z)$ denote error function and complementary error function about z, respectively. κ [m^2/s] denotes coolant thermal diffusivity and,

$$\begin{aligned} \phi &= q/\lambda, \\ \phi_s &= q_s/\lambda. \end{aligned} \tag{23}$$

The thermal properties are functions of the coolant temperature in the actual coolant. If $q_s = 0$, the calculated transient heat transfer coefficient should equal to the one calculated from Equation (18) under assumption of constant heat flux. Therefore, the thermal properties in the term which is not multiplied by q_s are treated as a function of

the coolant temperature. Since the transient heat transfer starts at $t = t_s$ actually, the time t in Equation (22) is substituted by $t - t_s$. Thus,

$$h_t = \left\{ 2\sqrt{\frac{t-t_s}{\pi\lambda\gamma}} - \frac{2q_s}{q}\sqrt{\frac{t-t_s}{\pi\lambda\gamma}}\left(1 - e^{-\frac{\gamma\delta_s^2}{4\lambda_s(t-t_s)}}\right) + \frac{\delta q_s}{\lambda_s q}\,\mathrm{erf}\left(\frac{\delta\sqrt{\gamma_s}}{2\sqrt{\lambda_s t}}\right)\right\}^{-1} . \quad (24)$$

Where γ_s[J/m^{3}K] and λ_s[W/mK] denote heat capacity and thermal conductivity of the coolant at $t = t_s$.

2.1.5 Properties of helium and copper and heating power

In POCHI1, independent variables are the density, mass flow rate and total internal energy. The thermal properties of the helium can be a function of the density and internal energy. The internal energy is a function of the independent variables, as follows.

$$e = E - \frac{\dot{m}^2}{2\rho} . \quad (25)$$

Therefore, the thermal properties of the helium can be calculated as a function of the independent variables through the relation of Equation (25). In POCHI1, the necessary region of the density and internal energy is dispersed and then, the thermal properties are previously calculated as a function of them on all of the lattices using a helium thermal properties calculation library[16]. During the simulation, the thermal properties are calculated by interpolating them to reduce the CPU time.

The electrical property of the copper is calculated as follows[17,18].

$$r = \mathrm{Max}(r_R, r_T) . \quad (26)$$

Where,

$$r_R = \begin{cases} r_0 & (B = 0), \\ r_0\left[1 + e^{-7.008+1.3831\ln(|B|\cdot RRR)-0.0298(\ln(|B|\cdot RRR))^2}\right] & (|B| > 0), \end{cases} \quad (27)$$

$$r_0 = \frac{1.553\times10^{-8}}{RRR} . \quad (28)$$

And,

$$r_T = r_0 + r_i + r_{i0}, \quad (29)$$

Where,

$$r_i = \frac{1.171\times10^{-17}\theta^{4.49}}{\left\{1 + 4.498\times10^{-7}\theta^{3.35}e^{-\left(\frac{50}{\theta}\right)^{6.428}}\right\}}, \quad r_{i0} = \frac{0.4531 r_0 r_i}{(r_0 + r_i)} \quad (30)$$

Note that effect of the magnetic field on the electric resistivity of the copper is ignored on the high temperature region because of luck of the magneto resistance measurement data.

The copper heat capacity is calculated from[17],

$$\log_{10}(\rho_{Cu}\gamma_{Cu}) = 1.131 - 9.454\log_{10}\theta + 12.99(\log_{10}\theta)^2 - 5.501(\log_{10}\theta)^3 + 0.7637(\log_{10}\theta)^4. \quad (31)$$

The copper thermal conductivity is[17],

$$\lambda_{Cu} = (W_0 + W_1 + W_{10})^{-1}. \quad (32)$$

Where,

$$W_0 = \frac{\beta}{\theta},\ W_1 = \frac{1.784\times10^{-8}\theta^{2.763}}{\left\{1+1.966\times10^{-5}\theta^{2.598}e^{\left(-\frac{70}{\theta}\right)^{1.756}}\right\}},\ W_{10} = \frac{pW_0W_1}{(W_0+W_1)} \quad (33)$$

$$p = \frac{0.838}{\beta_r^{0.1661}},\ \beta_r = \frac{\beta}{3\times10^{-4}},\ \beta = \frac{0.643}{RRR}. \quad (34)$$

The heating power deposited on the conductor is,

$$Q = Q_h + Q_J \quad (35)$$

$$Q_h = \begin{cases} E_h/t_h & (0 \le t \le t_h \cap x_{hl} \le x \le x_{hr}) \\ 0 & (t_h < t \cup x < x_{hl} \cup x_{hr} < x) \end{cases} \quad (36)$$

$$Q_J = g(\theta)Q_{Jf} \quad (37)$$

Where,

$$Q_{Jf} = \frac{rI_t^2}{A_{Cu}A_{st}}. \quad (38)$$

$$g(\theta) = \begin{cases} 0 & (\theta \le \theta_{cs}) \\ \dfrac{\theta-\theta_{cs}}{\theta_c-\theta_{cs}} & (\theta_{cs} \le \theta \le \theta) \\ 1 & (\theta_c \le \theta) \end{cases} \quad (39)$$

2.2 Finite differential scheme for the coolant

Implicit time-dependent differencing of Equation (8) is,

$$\frac{\boldsymbol{u}_i^{n+1}-\boldsymbol{u}_i^n}{\delta t} + \frac{\boldsymbol{F}_{i+1}^{n+1}-\boldsymbol{F}_{i-1}^{n+1}}{2\delta x} + \boldsymbol{G}_i^{n+1} = \boldsymbol{0}\ . \quad (40)$$

Since $\boldsymbol{F}^{n+1}$ and $\boldsymbol{G}^{n+1}$ are nonlinear functions of $\boldsymbol{u}^{n+1}$, it is obviously difficult to solve this equation. The non-linearity of this equation is then eliminated by following linearization procedure, which was applied by Beam and Warming[9]. A local Taylor expansion of $\boldsymbol{F}^{n+1}$ about $\boldsymbol{u}^{n+1}$ yields,

$$\boldsymbol{F}^{n+1} = \boldsymbol{F}^n + \boldsymbol{A}^n\left(\boldsymbol{u}^{n+1}-\boldsymbol{u}^n\right). \quad (41)$$

Where $\boldsymbol{A}$ denotes the Jacobian matrix, that is,

$$A = \frac{\partial F}{\partial u} = \begin{pmatrix} 0 & 1 & 0 \\ -u^2 + \frac{\partial P}{\partial \rho} & 2u + \frac{\partial P}{\partial \dot{m}} & \frac{\partial P}{\partial E} \\ u(\frac{\partial P}{\partial \rho} - \frac{E+P}{\rho}) & \frac{E+P}{\rho} + u\frac{\partial P}{\partial \dot{m}} & u(1+\frac{\partial P}{\partial E}) \end{pmatrix}. \tag{42}$$

$$u = \dot{m}/\rho \tag{43}$$

Since the coolant pressure is a function of the density and internal energy, the derivatives in Equation (42) should be replaced with the ones about the density and internal energy. Using Equation (25),

$$\begin{aligned} \frac{\partial P}{\partial \rho} &= \left.\frac{\partial P}{\partial \rho}\right|_e + \frac{u^2}{2}\left.\frac{\partial P}{\partial e}\right|_\rho, \\ \frac{\partial P}{\partial \dot{m}} &= -u\left.\frac{\partial P}{\partial e}\right|_\rho, \\ \frac{\partial P}{\partial E} &= \left.\frac{\partial P}{\partial e}\right|_\rho. \end{aligned} \tag{44}$$

Thus, one obtains,

$$A = \begin{pmatrix} 0 & 1 & 0 \\ u^2\left(-1 + \frac{1}{2}\frac{\partial P}{\partial e}\right) + \frac{\partial P}{\partial \rho} & u\left(2 - \frac{\partial P}{\partial e}\right) & \frac{\partial P}{\partial e} \\ u(\frac{\partial P}{\partial \rho} + \frac{u^2}{2}\frac{\partial P}{\partial e} - \frac{E+P}{\rho}) & \frac{E+P}{\rho} - u^2\frac{\partial P}{\partial e} & u(1+\frac{\partial P}{\partial e}) \end{pmatrix}. \tag{45}$$

On the other hand, G has a difficulty in its linearization since it has discontinuity from its definition. In addition, G originally has some error in the modeling process. For instance, the friction force is determined from a result in steady state measurement and then, the friction force due to compression or expansion of the fluid is ignored. Also, the heat transfer from the conductor to the coolant is approximately treated as shown in the previous section. Therefore, the precious treatment of G^{n+1} does not seem to be effective in comparison with its difficulties. G^{n+1} is then substituted by G^n to avoid the non-linearity of the system, for sake of simplicity, in this simulation. Consequently,

$$\frac{\delta t}{2\delta x} A_{i+1}^n u_{i+1}^{n+1} + I u_i^{n+1} - \frac{\delta t}{2\delta x} A_{i-1}^n u_{i-1}^{n+1} = v_i^n. \tag{46}$$

Where,

$$v_i^n = \frac{\delta t}{2\delta x} A_{i+1}^n u_{i+1}^n + I u_i^n - \frac{\delta t}{2\delta x} A_{i-1}^n u_{i-1}^n - \frac{\delta t}{2\delta x}(F_{i+1}^n - F_{i-1}^n) - \delta t G_i^n \tag{47}$$

This scheme offers second order spatial accuracy. In this scheme, forth order artificial dissipative term δu is added for stabilization[9]. The artificial dissipative term is,

$$\delta u_i = u_{i+2} - 4u_{i+1} + 6u_i - 4u_{i-1} + u_{i-2}. \tag{48}$$

And, $\boldsymbol{u}$ in Equation (47) is substituted by,

$$\bar{\boldsymbol{u}}_l = \boldsymbol{u}_l - \delta\boldsymbol{u}_l/16. \tag{49}$$

The boundary condition of this system is as follows. In general, there exists resistance for the flow before the coolant inlet and behind the outlet, such as a piping, a valve and so on. In POCHI1, the pressure drop by the resistance is assumed to be proportional to dynamic pressure. The pressure at the inlet and outlet are then calculated from,

$$\begin{aligned} P_{in}^{n+1} &= P_{in}' - C_{in}\frac{\left(\dot{m}_0^n\right)^2}{2\rho_0^n}, \\ P_{out}^{n+1} &= P_{out}' + C_{out}\frac{\left(\dot{m}_l^n\right)^2}{2\rho_l^n}. \end{aligned} \tag{50}$$

Where P_{in}' [MPa] and P_{out}' [MPa] denote constant pressure before the resistance at the inlet and behind the resistance at the outlet, respectively. In Equation (50), the dynamic pressures at the previous time step are used for sake of simplicity. The coolant temperature at the inlet is given in case that the coolant supplied from a coolant inlet. Then, the density and total internal energy can be calculated from,

$$\rho_0^{n+1} = \rho\left(T_{in}, P_{in}^{n+1}\right), \tag{51}$$

$$E_0^{n+1} = e\left(T_{in}, P_{in}^{n+1}\right) + \frac{\left(\dot{m}_0^{n+1}\right)^2}{2\rho\left(T_{in}, P_{in}^{n+1}\right)}. \tag{52}$$

Non-linearity of Equation (52) is removed according to the following procedure.

$$\left(\dot{m}^{n+1}\right)^2 = \left(\dot{m}^n + \delta\dot{m}\right)^2 \approx \left(\dot{m}^n\right)^2 + 2\delta\dot{m}\dot{m}^n = \dot{m}^n\left(2\dot{m}^{n+1} - \dot{m}^n\right). \tag{53}$$

The mass flow rate at the inlet is assumed to equal to the one at the neighbor point. Consequently, one has,

$$\boldsymbol{u}_0^{n+1} = \boldsymbol{B}^n\boldsymbol{u}_1^{n+1} + \boldsymbol{h}^n \tag{54}$$

Where,

$$\boldsymbol{B}^n = \begin{pmatrix} 0 & 0 & 0 \\ 0 & 1 & 0 \\ 0 & \dfrac{\dot{m}_0^n}{\rho\left(T_{in}, P_{in}\right)} & 0 \end{pmatrix}, \quad \boldsymbol{h}^n = \begin{pmatrix} \rho\left(T_{in}, P_{in}\right) \\ 0 \\ e\left(T_{in}, P_{in}\right) - \dfrac{\left(m_0^n\right)^2}{2\rho\left(T_{in}, P_{in}\right)} \end{pmatrix}. \tag{55}$$

If the coolant is expelled from the inlet as a result of heating in the conductor, the boundary condition at the inlet is[8,9],

$$\boldsymbol{u}_0^{n+1} = \boldsymbol{u}_1^{n+1} \tag{56}$$

The boundary condition at the outlet is[8,9],

$$\boldsymbol{u}_l^{n+1} = \boldsymbol{u}_{l-1}^{n+1} \tag{57}$$

Equations (46), (54) or (56) and (57) can be solved without iterations since it is a block

tridiagonal system. Thus, the CPU time can be greatly reduced.

The initial condition is a convergent solution of Equations (46), (54) and (57) under condition of no heat generation from the conductor.

2.3 Finite differential equation for the conductor

Implicit finite-difference scheme for Equation (6) is,

$$\gamma_{st}\frac{\theta_i^{n+1}-\theta_i^n}{\delta t}=\frac{A_{Cu}\lambda_{Cu}}{A_{st}}\frac{\theta_{i+1}^{n+1}-2\theta_i^{n+1}+\theta_{i-1}^{n+1}}{\delta x^2}+\frac{A_{Cu}}{A_{st}}\left(\frac{\partial\lambda_{Cu}}{\partial x}\right)_i^n\frac{\theta_{i+1}^{n+1}-\theta_{i-1}^{n+1}}{2\delta x}$$
$$-\frac{h_i^n Pe}{A_{st}}(\theta_i^{n+1}-T_i^{n+1})-\frac{A_c\gamma_c}{A_{st}}\frac{T_i^{n+1}-T_i^n}{\delta t}+g(\theta_i^{n+1})(Q_{Jf})_i^n. \tag{58}$$

Note that the values at a previous time step are used for $\partial\lambda_{Cu}/\partial x$, h and Q_{Jf} to make the equation more stable. Equation (58) is solved by S.O.R method[8].

Boundary conditions for this system are adiabatic condition in the longitudinal direction, that is,

$$\left.\frac{\partial\theta}{\partial x}\right|_{x=0}=\left.\frac{\partial\theta}{\partial x}\right|_{x=L}=0. \tag{59}$$

Initial condition is,

$$\theta_i^0=T_i^0. \tag{60}$$

3. Comparison with Experiment Results

The verification of the code is carried out by comparing simulation results with experimental results of normal zone propagation behavior measured with two samples of CIC conductors

Table 1 Main parameters of sample 1 and 2

	Sample 1	Sample 2
Superconductor	NbTi	NbTi
Strand number	48	27
Strand diameter	0.832 mm	1.105 mm
NbTi : Cu : CuNi	1 : 3.88 : 1.07	1 : 3.88 : 1.07
Void fraction	36.8%	36.0%
Hydraulic diameter	0.43 mm	0.53 mm
Electrical resistivity at 7 T	6.25 Ωm	6.25 Ωm
Conductor length	6 m	6 m
Inner diameter of conduit	7.41 mm	7.41 mm
Outer diameter of conduit	9.61 mm	9.61 mm

3.1 Experimental results

Main parameters of the samples are summarized in *Table 1*. The number of the strands and their diameter are different, but the cross-sectional area of NbTi, Cu ,CuNi and helium are almost the same. The difference of the strands number and diameter reflects on hydraulic diameter and cooling perimeter. The conductor is wound into a helix with 180 mm diameter and impregnated with epoxy resin for reinforcement and thermal insulation. *Figure 5 (a)* shows the configuration of the samples.

The samples were installed in the backup coil in liquid helium (LHe) and subjected to the magnetic field of 7 T. The conductors were cooled by making SHe forcibly flow in them. *Figure 5 (b)* shows the test arrangement. The initial normalcy was originated by supplying 1 kHz sinusoidal wave current to the inductive heater attached on the conductor. The heating duration was 10 ms and length of the inductive heater was 10 cm. The normal zone propagation length was evaluated from voltage signals measured between taps. The location of the voltage taps is shown in *Figure 5 (c)*.

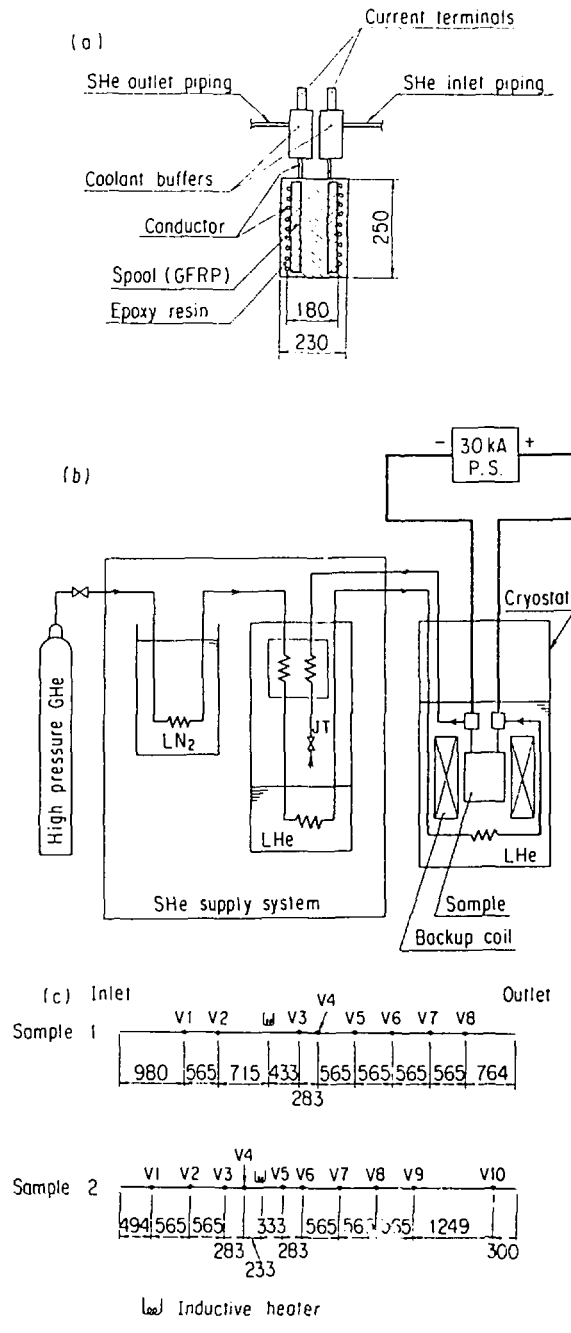

Figure 5. (a) Configuration of the samples. (b) Construction of sample and equipment to supply SHe to the sample. (c) Location of the voltage taps.

Table 2 Experimental condition

	Sample 1	Sample 2
Magnetic field	7 T	7 T
Transport current	3000 A	2800 A
Initial coolant pressure	6.0 atm	5.8 atm
Initial coolant flow rate	0.47 g/s	0.51 g/s
initial coolant temperature	4.28 K	4.28 K
Heating duration	10 ms	10 ms

Experimental conditions are shown in *Table* 2. The voltage profiles observed during the normal zone propagation are shown in *Figures 6* and *7*. The normal zone propagation length in both upstream and downstream directions from heating center were measured in each samples.

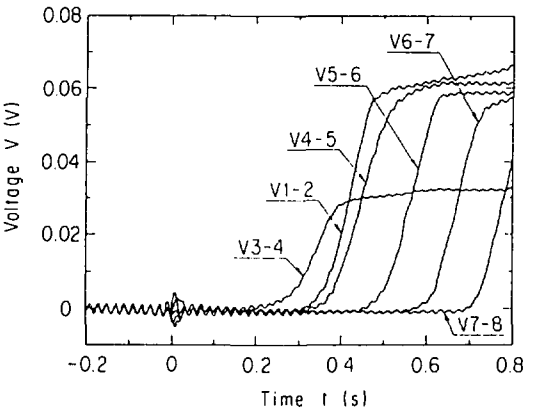

Figure 6. Voltage profile during the normal zone propagation in the sample 1.

3.2 Simulation results

Since the superconductor of the samples is NbTi, γ_{sc} is calculated from a reference 19. The strand includes CuNi, so γ_{el} should be defined. γ_{Cu} substitutes for γ_{el}, for simplicity. γ_c is calculated from an equation in a reference 20 since the conduit are made from stainless steel. Critical temperature is calculated from a reference 21, and current sharing temperature is evaluated by linear interpolation of the critical current and the critical temperature. The parameters

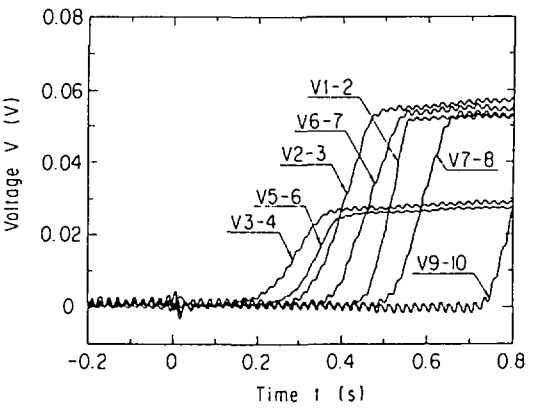

Figure 7. Voltage profile during the normal zone propagation in the sample 2.

Table 3 Parameters in simulations

	Sample 1	Sample 2
Discrete length increment	5 mm	5 mm
Number of grids	1201	1201
Discrete time increment	0.5 ms	0.5 ms
Number of time steps	1601	1601
Critical temperature	6.21 K	6.21 K
Current sharing temperature	4.80 K	4.89 K
Input energy	2.42×10^4 J/m^3	2.96×10^4 J/m^3
(C_{in}, C_{out})	(0,0) and (500,500)	(0,0) and (500,500)

used in the simulations are shown in *Table 3*. The other parameters are the ones indicated in *Tables 1* and *2*.

The calculations were performed by FUJITSU VP2600, whose performance is 5 GFlops. The CPU time were less than 10 minutes for each calculation. The CPU time seems to be short for the quench simulation for 800 ms with the 1201 lattices whose discrete increment is 5 mm.

3.2.1 Normal zone propagation length

The calculation was carried out for $(C_{in}, C_{out}) = (0,0)$ and $(500,500)$. The former case corresponds to the constant inlet and outlet pressure condition. The calculated normal zone propagation length in the upstream and downstream directions from the heating center is shown in *Figures 8* and *9* with the measured results. In case of $(C_{in}, C_{out}) = (0,0)$, the upstream normal zone propagates faster than the downstream although they were almost same in the measurement. However, the simulation result indicates that the existence of the flow resistance makes the difference between the upstream and downstream normal zone propagation length to be smaller but they shift little as a whole. It is then expected the difference of the flow resistance reflects on merely the deviation between the upstream and downstream normal zone propagation length, at least, below the flow resistance level of $(C_{in}, C_{out}) = (500,500)$.

The samples have coolant buffers at their coolant inlet and outlet. However, the coolant in them seems to have almost no compressibility in these coolant buffers, since the temperature of it equals to the bath temperature and then, is much lower than pseudocritical temperature of 7.2K. Therefore, the coolant buffers do not play a role to keep the pressure to be constant. The piping and valves before the inlet and behind the outlet, consequently, cause the flow resistance.

The magnitude of the flow resistance was not estimated in this experiment. However,

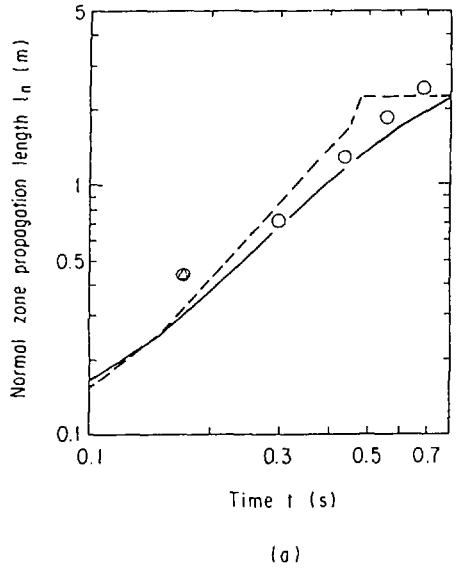

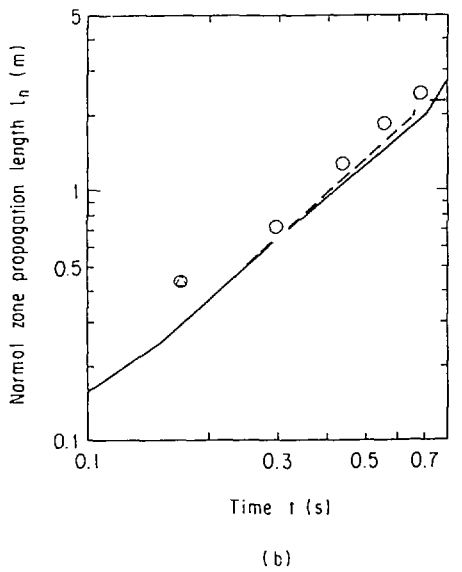

Figure 8. Normal zone propagation length in the sample 1. The open circle and triangle indicate the measured normal zone length in the downstream and upstream directions, respectively. The solid and broken lines are the simulated downstream and upstream normal zone propagation lengths. (a) $(C_{in},C_{out}) = (0,0)$. (b) $(C_{in},C_{out}) = (500,500)$.

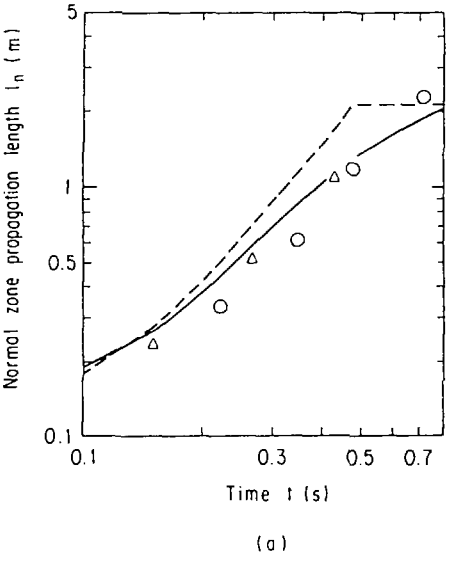

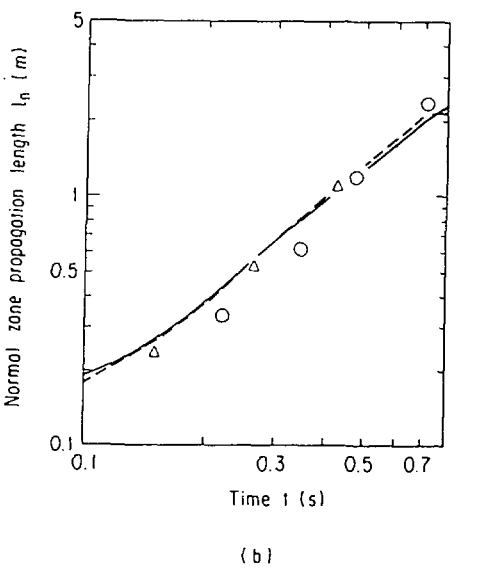

Figure 9. Normal zone propagation length in the sample 2. The open circle and triangle indicate the measured normal zone length in the downstream and upstream directions, respectively. The solid and broken lines are the simulated downstream and upstream normal zone propagation lengths. (a) $(C_{in},C_{out}) = (0,0)$. (b) $(C_{in},C_{out}) = (500,500)$.

the measured pressure rise at the coolant outlet is smaller than the one simulated for $(C_{in}, C_{out}) = (500,500)$. This indicates the flow resistance of the samples is smaller than 500. Then, the flow resistance of the samples is thought to be between $(C_{in}, C_{out}) = (0,0)$ and $(500,500)$. Moreover, the deviation between the upstream and downstream normal zone propagation length was small in the measurement ,so that the flow resistance in the samples is thought to be closer to $(C_{in}, C_{out}) = (500,500)$. The simulated results for $(C_{in}, C_{out}) = (500,500)$ show relatively good agreement with the measured although increment of the normal zone length in the experiment is larger than in the simulation.

3.2.2 Voltage behavior

Figure 10 shows the voltage behavior simulated for the sample 1 test. The increase of the measured normal voltage is slower than the simulated one at the beginning of the normal transition. One possible interpretation of the slow increment of the normal voltage is as follows. The complex geometry of the CIC conductor makes the coolant flow strongly disturbed. Then, the heat transfer performance in the turbulent region can be better than the one estimated by Equation (17). When very good heat transfer performance can be obtained, the strand temperature becomes equal to the coolant temperature. In this case, the normal voltage appears when the temperature of the coolant flowed out of the heated region reaches the current sharing temperature, and it gradually increases until this coolant temperature becomes the critical temperature. Also, the voltage increases after full normal transition in the measurement although the plateau appears in the simulated voltage. This indicates the estimation of the electric resistivity on the high temperature region is underestimation. In addition, this interprets the discrepancy in the normal propagation velocity between the measured and the simulated. It is therefore ex

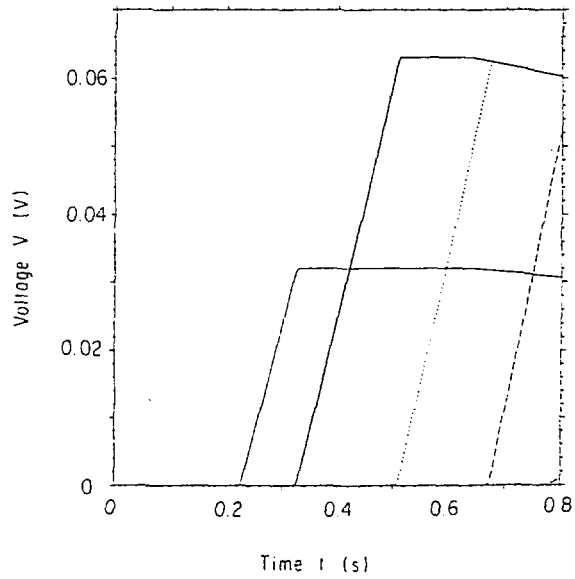

Figure 10. Simulated voltage profile in the sample 2. A solid, bold, dot, broken and dot-dash lines indicate the voltage profile for V3-4, V4-5, V5-6, V6-7 and V7-8.

pected the simulation of the normal zone propagation length for the actual flow resistance will also show good agreement with the measured.

4. Conclusion

The new quench simulation code, POCHI1, is developed. In POCHI1, the restriction from the CFL condition can be eliminated by applying implicit-time dependent finite different scheme. Moreover, the CPU time for quench simulation could be reduced since a tridiagonal system, which needs no iterations for solution, was offered for the fluid dynamics finite difference equation as a result of linearilzation of it. The simulation results was compared with the experiment results of the normal zone propagation in the two different CIC conductor samples. Normal zone propagation length shows relatively good agreement. However, it seems to be necessary to improve the treatment of the heat transfer coefficient in the turbulent region and the electric resistivity of the copper stabilizer in the high temperature region. The code will be improved near future.

Acknowledgment

The authors would like to thank Drs. S. Tamura and M. Yoshikawa for their encouragement and support during this work. Authors would also like to thank to all the staff of the Superconducting Magnet Laboratory and Computing and Information Systems Center in Japan Atomic Energy Research Institute.

Reference

1 **Benkowitsch, J. and Krafft G.** *Cryogenics* (1980) **20** 209

2 **Junghans, D.** *Cryogenics* (1983) **23** 220

3 **Marinucci, C.** *Cryogenics* (1983) **23** 579

4 **Kamitani, A., Amano, T., Sekiya, S. and Ohara, A.** *Cryogenics* (1991) **31** 110

5 **Agatsuma, K.** *Cryogenics* (1991) **31** 551

6 **Cheng, X.** *Cryogenics* (1994) **34** 195

7 **Shajii, A. and Freidberg, J.** *J. Applied Physics* To be published

8 **Roache, P.** Computational Fluid Dynamics Hermosa Publishers Inc. USA (1976)

9 **Beam, R and Warming, R.** *Journal of Computational Physics* (1976) **22** 87

10 **Koizumi, N, Takahashi, Y., Sugimoto, M, Hamada, K., *et al.*** JAERI-M (1994) *To be published.*

11 **Lue, J., Miller, J. and Lottin, J.** *IEEE Trans. on Magnet* (1979) **MAG-15** 53

12 **Tada, E., Takahashi, Y., Tsuji, H., Okuno, K. *et al.*** *Cryogenics* (1991) **32** 829

13 **Bloem, W.** *Cryogenics* (1986) **26** 300

14 **Carslow, H. and Jaeger, J.** *Conduction of Heat in Solids* Clarendon Press, Oxford, UK (1950)

15 **Steward, W.** *Int J. Heat Mass Transfer* (1978) **Vol. 21** 863

16 **Arp, V. and McCarty, R.** *Thermophysical Properties of Helium-4 From 0.8 to 1500 K With Pressures to 2000 MPa*, NIST Tech Note 1334 US Government Printing Office, Washington, USA (1989)

17 **Simon, J., Drexler, E. and Reed R.** *Properties of Copper and Copper Alloys at Cryogenic Temperatures NIST Monograph 177*, US Government Printing Office, Washington, USA, (1992)

18 *Handbook on Materials for Superconducting Machinery* NBS MCIC-HB-04 (1974)

19 **Bishoff, J., Vassilev, P. and Goncharov, I.** *Cryogenics* (1982) **22** 131

20 *Structural Materials for Superconducting Magnets*, NBS AISI 304 Stainless Steel, (1985) 304-50

21 **Spencer, C., Sanger, P. and Young, M.** *IEEE Trans. Magn.* (1979) **MAG-15** 76

国際単位系 (SI) と換算表

表1　SI基本単位および補助単位

量	名称	記号
長さ	メートル	m
質量	キログラム	kg
時間	秒	s
電流	アンペア	A
熱力学温度	ケルビン	K
物質量	モル	mol
光度	カンデラ	cd
平面角	ラジアン	rad
立体角	ステラジアン	sr

表2　SIと併用される単位

名称	記号
分，時，日	min，h，d
度，分，秒	°，′，″
リットル	l，L
トン	t
電子ボルト	eV
原子質量単位	u

1 eV = 1.60218 × 10^{-19} J

1 u = 1.66054 × 10^{-27} kg

表3　固有の名称をもつSI組立単位

量	名称	記号	他のSI単位による表現
周波数	ヘルツ	Hz	s^{-1}
力	ニュートン	N	m·kg/s^2
圧力，応力	パスカル	Pa	N/m^2
エネルギー，仕事，熱量	ジュール	J	N·m
工率，放射束	ワット	W	J/s
電気量，電荷	クーロン	C	A·s
電位，電圧，起電力	ボルト	V	W/A
静電容量	ファラド	F	C/V
電気抵抗	オーム	Ω	V/A
コンダクタンス	シーメンス	S	A/V
磁束	ウェーバ	Wb	V·s
磁束密度	テスラ	T	Wb/m^2
インダクタンス	ヘンリー	H	Wb/A
セルシウス温度	セルシウス度	℃	
光束	ルーメン	lm	cd·sr
照度	ルクス	lx	lm/m^2
放射能	ベクレル	Bq	s^{-1}
吸収線量	グレイ	Gy	J/kg
線量当量	シーベルト	Sv	J/kg

表4　SIと共に暫定的に維持される単位

名称	記号
オングストローム	Å
バーン	b
バール	bar
ガル	Gal
キュリー	Ci
レントゲン	R
ラド	rad
レム	rem

1 Å = 0.1 nm = 10^{-10} m

1 b = 100 fm^2 = 10^{-28} m^2

1 bar = 0.1 MPa = 10^5 Pa

1 Gal = 1 cm/s^2 = 10^{-2} m/s^2

1 Ci = 3.7 × 10^{10} Bq

1 R = 2.58 × 10^{-4} C/kg

1 rad = 1 cGy = 10^{-2} Gy

1 rem = 1 cSv = 10^{-2} Sv

表5　SI接頭語

倍数	接頭語	記号
10^{18}	エクサ	E
10^{15}	ペタ	P
10^{12}	テラ	T
10^{9}	ギガ	G
10^{6}	メガ	M
10^{3}	キロ	k
10^{2}	ヘクト	h
10^{1}	デカ	da
10^{-1}	デシ	d
10^{-2}	センチ	c
10^{-3}	ミリ	m
10^{-6}	マイクロ	μ
10^{-9}	ナノ	n
10^{-12}	ピコ	p
10^{-15}	フェムト	f
10^{-18}	アト	a

（注）

1. 表1～5は「国際単位系」第5版，国際度量衡局 1985年刊行による．ただし，1 eVおよび1 uの値はCODATAの1986年推奨値によった．
2. 表4には海里，ノット，アール，ヘクタールも含まれているが日常の単位なのでここでは省略した．
3. barは，JISでは流体の圧力を表わす場合に限り表2のカテゴリーに分類されている．
4. EC閣僚理事会指令ではbar，barnおよび「血圧の単位」mmHgを表2のカテゴリーに入れている．

換　算　表

力	N(=10^5 dyn)	kgf	lbf
	1	0.101972	0.224809
	9.80665	1	2.20462
	4.44822	0.453592	1

粘度　1 Pa·s(N·s/m^2) = 10 P(ポアズ)(g/(cm·s))

動粘度　1 m^2/s = 10^4 St(ストークス)(cm^2/s)

圧力	MPa(=10 bar)	kgf/cm^2	atm	mmHg(Torr)	lbf/in^2(psi)
	1	10.1972	9.86923	7.50062 × 10^3	145.038
	0.0980665	1	0.967841	735.559	14.2233
	0.101325	1.03323	1	760	14.6959
	1.33322 × 10^{-4}	1.35951 × 10^{-4}	1.31579 × 10^{-3}	1	1.93368 × 10^{-2}
	6.89476 × 10^{-3}	7.03070 × 10^{-2}	6.80460 × 10^{-2}	51.7149	1

エネルギー・仕事・熱量	J(=10^7 erg)	kgf·m	kW·h	cal(計量法)	Btu	ft·lbf	eV
	1	0.101972	2.77778 × 10^{-7}	0.238889	9.47813 × 10^{-4}	0.737562	6.24150 × 10^{18}
	9.80665	1	2.72407 × 10^{-6}	2.34270	9.29487 × 10^{-3}	7.23301	6.12082 × 10^{19}
	3.6 × 10^6	3.67098 × 10^5	1	8.59999 × 10^5	3412.13	2.65522 × 10^6	2.24694 × 10^{25}
	4.18605	0.426858	1.16279 × 10^{-6}	1	3.96759 × 10^{-3}	3.08747	2.61272 × 10^{19}
	1055.06	107.586	2.93072 × 10^{-4}	252.042	1	778.172	6.58515 × 10^{21}
	1.35582	0.138255	3.76616 × 10^{-7}	0.323890	1.28506 × 10^{-3}	1	8.46233 × 10^{18}
	1.60218 × 10^{-19}	1.63377 × 10^{-20}	4.45050 × 10^{-26}	3.82743 × 10^{-20}	1.51857 × 10^{-22}	1.18171 × 10^{-19}	1

1 cal = 4.18605 J(計量法)

= 4.184 J　(熱化学)

= 4.1855 J　(15 ℃)

= 4.1868 J(国際蒸気表)

仕事率　1 PS(仏馬力)

= 75 kgf·m/s

= 735.499 W

放射能	Bq	Ci
	1	2.70270 × 10^{-11}
	3.7 × 10^{10}	1

吸収線量	Gy	rad
	1	100
	0.01	1

照射線量	C/kg	R
	1	3876
	2.58 × 10^{-4}	1

線量当量	Sv	rem
	1	100
	0.01	1

(86年12月26日現在)

IMPLICIT TIME-DEPENDENT FINITE DIFFERENT ALGORITHM FOR QUENCH SIMULATION